THE UNIVERSITY OF RHODE ISLAND

University of Rhode Island
DigitalCommons@URI

Chemical Engineering Faculty Publications | Chemical Engineering

2022

PFAS fluidize synthetic and bacterial lipid monolayers based on hydrophobicity and lipid charge

Aleksandra Naumann
University of Rhode Island

Jessica Alesio
University of Rhode Island

Monika Poonia
University of Rhode Island

Geoffrey D. Bothun
University of Rhode Island, gbothun@uri.edu

Follow this and additional works at: https://digitalcommons.uri.edu/che_facpubs

The University of Rhode Island Faculty have made this article openly available.
Please let us know how Open Access to this research benefits you.

This is a pre-publication author manuscript of the final, published article.

Terms of Use

This article is made available under the terms and conditions applicable towards Open Access Policy Articles, as set forth in our Terms of Use.

Citation/Publisher Attribution

Maumann, A., Alesio, J., Poonia, M., & Bothun, G. D. (2022). PFAS fluidize synthetic and bacterial lipid monolayers based on hydrophobicity and lipid charge. *Journal of Environmental Chemical Engineering, 10*(2), 107351. https://doi.org/10.1016/j.jece.2022.107351
Available at: https://doi.org/10.1016/j.jece.2022.107351

This Article is brought to you for free and open access by the Chemical Engineering at DigitalCommons@URI. It has been accepted for inclusion in Chemical Engineering Faculty Publications by an authorized administrator of DigitalCommons@URI. For more information, please contact digitalcommons@etal.uri.edu.

PFAS fluidize synthetic and bacterial lipid monolayers based on hydrophobicity and lipid charge

*Aleksandra Naumann[1], Jessica Alesio[1], Monika Poonia[1], and Geoffrey D. Bothun[1,]**

Department of Chemical Engineering, University of Rhode Island, 2 East Alumni Ave, Kingston, RI, 02881

*Corresponding Author. Tel: +1-401-874-9517, Fax: +1-401-874-2656, E-mail: gbothun@uri.edu

KEYWORDS: Perfluoroalkyl substance; perfluorooctanoic acid; lipid monolayer; surface pressure; bacteria membrane

Abstract

Poly- and Perfluoroalkyl substances (PFASs) are pollutants of emerging concern that persist in nature and pose environmental health and safety risks. PFAS disrupt biological membranes resulting in cellular inhibition, but the mechanism of disruption and the role of lipid composition remain unclear. We examine the role of phospholipid saturation and headgroup charge on the interactions between PFASs and phospholipid monolayers comprised of synthetic phosphocholine (PC) and phosphoglycerol (PG) lipids and prepared from bacteria membrane extracts rich in PG lipids from an environmentally relevant marine bacterium *Alcanivorax*

borkumensis. When deposited on a buffered subphase containing PFAS, PFAS mixed within and fluidized zwitterionic and net-anionic monolayers leading to increases in monolayer compressibility that were driven by a combination of PFAS hydrophobicity and monolayer charge density. Differences in the monolayer response using saturated or unsaturated lipids are attributed to the ability of the unsaturated lipids to accommodate PFAS within 'void space' arising from the bent lipid tails. Similar fluidization and compressibility behavior were also observed in *A. borkumensis* lipid monolayers. This work provides new insight into PFAS partitioning into bacterial membranes and the effect PFAS have on the physicomechanical properties of zwitterionic and charged lipid monolayers.

1. Introduction

Poly- and Perfluoroalkyl substances (PFAS) are pollutants of emerging concern that exhibit an unprecedented ability to accumulate within the environment.[1–3] PFAS, which are fluorinated amphiphiles with low volatility, have been used in a wide range of products and processes where low adhesion and water and oil repellency are required.[4,5] These properties also cause PFAS to persist in the environment and bioaccumulate. For example, one of the most-studied PFAS, perfluorooctanesulfonic acid (PFOS) is known to be present in blood serum of US citizens at concentrations near 40 ng/mL.[6] In addition, the short-chain PFAS perfluorobutanesulfonic acid (PFBS) found in cord blood was positively associated with preeclampsia.[7] Even years after exposure, high levels of PFAS remain in the body.[8,9] Although there has been a shift to PFAS with shorter fluorinated tails that are thought to bioaccumulate to a lesser extent than longer PFAS, compounds with long fluorinated tails ($C_{nF} \geq 7$) remain in the environment, even in remote areas such as the arctic through the global water cycle.[6,10,11]

PFAS bioaccumulation has been linked to lipid and protein binding mechanisms, consistent with the hydrophobic nature of the compounds.[12–15] While there have been numerous studies focused on PFAS-protein binding, comparably few studies have focused on PFAS partitioning into lipid bilayer membranes or monolayers.[16–22] Perfluorooctanoic acid (PFOA) and PFOS, legacy eight-carbon PFASs, have been shown to readily partition into bilayers comprised of zwitterionic phospholipids, disrupting inter-lipid interactions and disordering the bilayer.[16,21,22] Interestingly, PFOA partitioning was dependent on phospholipid chain length[22] while PFOS partitioning was not,[16] which may reflect the greater hydrophobicity of PFOS. Even short chain PFAS such as PFBS partition into and disrupt zwitterionic phospholipid bilayers.[17,18]

Phospholipid monolayer studies provide additional insight into PFAS partitioning and its effects on physicomechanical monolayer properties. PFOA, PFOS and PFBS have been shown to partition into zwitterionic phospholipid monolayers.[18–20] As the monolayers were compressed, packing the lipids more closely together and increasing the inter-lipid interactions, PFOA was expelled from the monolayer while the sulfonic acids PFOS[19,20] and PFBS[18] were retained. Collectively, previous work such as these show that bilayer and monolayer studies provide complimentary information that can be combined to better understand how lipid partitioning varies with PFAS and lipid composition.

Bacteria have a central function in ecosystems, and it is critical to understand how PFAS partition into and disrupt bacterial cell membranes. Previous studies have shown that PFAS partitioning into *Staphylococcus epidermidis* and *Aliivibrio fischeri* was dependent on PFAS hydrophobicity,[23] determined largely by fluorinated tail length. While the general behavior for bacteria partitioning with PFAS hydrophobicity agreed with partitioning observed with zwitterionic phospholipid bilayers, lower PFAS partition coefficients for bacteria were attributed

to electrostatic repulsion between PFASs and the negatively charged bacterial membrane. With *A. fischeri* the membranes become more permeable after PFAS exposure, which may have contributed to increased quorum sensing.[24] PFOA and PFOS have also been shown to disrupt *Escherichia coli* membranes, contributing to toxicity[25] and increasing biofilm formation as a stress response to the added PFAS.[26]

The objective of this work was twofold; (1) to examine the effect of phospholipid tail saturation and charge on PFAS interactions within monolayers and (2) to determine if these interactions are also observed in monolayers comprised of lipids extracted from *Alcanivorax borkumensis*. Saturated and mono-unsaturated phosphocholine (PC) and phosphoglycerol (PG) lipids were chosen to represent bacterial lipids. *A. borkumensis* was employed as a model organism. It is a ubiquitous marine bacterium known for its ability to utilize alkanes as a carbon source and is often found to be a dominant species in association with marine oil spills.[27,28] The primary lipid fatty acids of *A. borkumensis* grown on the same carbon source employed in this work – saturated C_{16} tails (16:0, ~30%) and mono-unsaturated C_{18} tails (18:1 Δ9-*cis*, ~40%)[29] – are similar to the tail structures used in the monolayer studies. The results show that phenomena observed in synthetic lipid monolayers also describe PFAS interactions in complex bacterial membrane extracts.

2. Experimental

2.1. Chemicals

Perfluorooctanoic acid (PFOA), perfluorononanoic acid (PFNA), perfluorooctanesulfonic acid (PFOS, potassium salt), and perfluorohexanesulfonic acid (PFHxS, sodium salt) were purchased from AccuStandard® (New Haven, CT) with purities > 96%. The phospholipids 1,2-

dimyristoyl-*sn*-glycero-3-phosphocholine (DMPC), 1,2-dimyristoyl-*sn*-glycero-3-phosphoglycerol (DMPG, sodium salt), 1,2-dioleoyl-*sn*-glycero-3-phosphocholine (DOPC), and 1,2-dioleoyl-*sn*-glycero-3-phosphoglycerol (DOPG, sodium salt) were purchased from Avanti® Polar Lipids (Alabaster, AL). All the materials were used as received without further purification. Experiments were conducted in 10 mM N-(2-hydroxyethyl)piperazine-N′-(2-ethanesulfonic acid) (HEPES, Sigma-Aldrich) buffer at pH 7 prepared using sterile, ultrafiltered deionized water (DIW) obtained from a Millipore Direct-3Q purification system. Molecular properties of the PFAS and phospholipids – the number of carbons (C_{nF} and C_n:cis), charge, octanol/water partition coefficient (Log K_{ow}), van der Waals volume (V_{vdw}), and polar surface area (A_{polar}) – are summarized in Table 1.

Table 1. Molecular properties of PFAS and phospholipid compounds.

Compound	C_{nF} (C_n)[b]	Charge	Log K_{ow}[d]	V_{vdw} (Å^3)[e]	A_{polar} (Å^3)[e]
PFASs					
PFOA	7 (8)	-	3.10 *(5.68)*	231	40
PFNA[a]	8 (9)	-	3.54 *(6.51)*	258	40
PFHxS[a]	6 (6)	-	2.20 *(3.39)*	221	57
PFOS	8 (8)	-	5.61 *(5.77)*	275	57
	C_n:cis[c]	Charge		V_{vdw} (Å^3)[e]	A_{polar} (Å^3)[e]
Lipids					
DMPC	14:0	-/+		716	111
DMPG	14:0	-		682	152
DOPC	18:1	-/+		836	111
DOPG	18:1	-		803	152

[a]Restricted to bacterial lipid monolayer studies.
[b]C_{nF} = number of fluorinated carbons; C_n = total number of carbons.
[c]C_n:cis = ratio of the total number of carbons to the number of double bonds in the tails.
[d]K_{ow} = octanol/water partition coefficient, experimental average *(predicted average)*, US EPA CompTox Chemicals Dashboard.[30]
[e]Computed with Marvin Sketch (Version 20.11).

2.2. Bacteria growth and lipid extraction

A. borkumensis was grown on 5 g/L pyruvate in artificial seawater at 20 °C. Details are provided in Supplementary Material for bacteria growth and lipid extraction. Briefly, bacteria were grown in sterile 125 mL baffled Erlenmeyer flasks for 72 h on the platform shaker at ambient temperature.[27] Cells were grown to an optical density, OD_{600}, of 1.2 and visually examined under a microscope (Figure S1). The bacteria were centrifuged at 7000 g for 30 min to form a pellet, which was then resuspended and washed twice with artificial seawater via centrifugation. For the final resuspension, the bacteria were pelletized again and resuspended in 2 mL 0.9% NaCl (w/w). Lipid extraction was achieved using a modified Bligh and Dyer method.[31,32] A total of 9 pellets (9 bacteria cultures) yielded an average of 3.52 ± 0.74 mg of extracted lipids per pellet, which were pooled for the monolayer studies (Figure S2, S3; Table S1).

2.3. Surface pressure measurements and Langmuir isotherms

The Langmuir isotherms were obtained using a PTFE trough (KSV NIMA, Biolin Scientific) measuring 364×75×4 mm (L×W×H) with a total working surface area of 240 cm^2 (see Figure S4 for an overview). The trough was placed on an air table (model Onyx 7A, Herzan, Laguna Hills, CA) for passive vibration control. All experiments were conducted at 20 °C with a 10 mM HEPES aqueous subphase. Prior to forming a Langmuir monolayer, the trough and barriers were rinsed thoroughly with ethanol three times and then the trough was filled with the aqueous subphase. The trough was considered sufficiently clean if the fluctuations in surface pressure at the neat air/water interface were less than 0.3 mN/m as the barriers were compressed down to 20-30% of the working surface area. Surface pressure was continuously measured using paper Wilhelmy plates (Nanoscience Instruments, Phoenix, AZ).

Lipid monolayers were formed by spreading small droplets of lipids dissolved in chloroform (1 g/L) on the surface of the aqueous subphase (with or without added PFAS) using a 50 µL Hamilton microsyringe. The chloroform was allowed to evaporate over 15 min. The surface pressure-area (π–Ā, where Ā is the mean molecular area or π–A, where A is the total trough area) isotherms were recorded by compressing the monolayers with a barrier speed of 3 mm/min, which allowed the monolayer to reach a pseudo-equilibrium condition. Surface pressure was recorded every 10 s using an integrated balance. Ā was calculated based on the total number of lipid molecules deposited at the air/water interface divided by the initial area of the trough. Brewster Angle Microscope (MicroBAM, KSV NIMA, Biolin Scientific) was used to image the monolayers *in situ*.

Compressibility moduli, C_s^{-1}, or the reciprocal of the compressibility, were calculated from the monolayer isotherms according to equation 1.

$$C_s^{-1} = -\bar{A}\frac{d\pi}{d\bar{A}} \qquad (1)$$

C_s^{-1} describes how resistant a monolayer is to compression; high values of C_s^{-1} correspond to a rigid monolayer with high resistance to compression, while low values of C_s^{-1} correspond to a fluid monolayer that requires less force to compress. The equation can also be applied when the area is the total trough area, A.

The surface activity of PFAS (no lipid present) were examined under compression by adding PFAS to the subphase and allowing the system to equilibrate for 15 min. PFAS monolayers were then compressed and recorded as they were for lipid monolayers. Lipid isotherms and PFAS surface pressure measurements were conducted in triplicate and the results are presented as the mean surface pressure. For ease of viewing, symbols were added

representing the mean value at every 50th data point. Standard error is shown in all figures as a lighter colored band around the mean.

3. Results and Discussion

Surface pressure–area (π–A) measurements for PFAS were generated to determine their surface activity at a bulk subphase concentration of 10^{-4} M (Figure S5). PFAS are soluble in water and upon compression the results reflect a competition between PFAS packing at the air/water interface and the adsorption energy. PFOA exhibited an s-shaped curve with π increasing from 4.2 to 11.5 mN/m with compression as PFOA packed more tightly at the interface and reduced the interfacial tension. PFOS exhibited a flat curve with comparatively high π between ~14–16 mN/m. In this case the surface was saturated with PFOS and the results suggests that PFOS molecules were expelled from the interface during compression, maintaining a near-constant surface pressure. The higher surface activity of PFOS compared to PFOA is consistent with PFOS being more hydrophobic based on Log K_{ow} (Table 1; comparison of experimental averages).[33] The range of π at the same PFAS concentrations are similar to previous work.[34,35] Estimated effective mean PFAS molecular areas ($\bar{A}_P$) were extrapolated from Schaefer et al[34] and Costanza et al[35] and are compared to computed minimum and maximum molecular area projections (Table 2). This comparison suggests that PFOS formed a packed monolayer oriented perpendicular to the air/water interface while PFOA formed a sparser monolayer with a higher degree of parallel orientation.

Table 2. Estimated and computed effective mean PFAS molecular areas.

Compound	Estimated $\bar{A}_P$ (Å^2)	Computed $\bar{A}_{P,min}$ (Å^2)[c]	Computed $\bar{A}_{P,max}$ (Å^2)[c]
PFOA	83[a], 181[b]	36	67

PFOS	55[a], 65[b]	37	77

[a]Extrapolated from Schaefer et al.[34]
[b]Extrapolated from Costanza et al.[35]
[c]Computed with Marvin Sketch (Version 20.11).

3.1. Saturated Phospholipid Monolayers (DMPC and DMPC/DMPG)

Isotherms were measured for DMPC/DMPG monolayers deposited on aqueous subphases with and without PFAS as a function of the anionic DMPG mole fraction (X_{DMPG} = 0, 0.15, and 0.3; Figure 1). With increasing X_{DMPG}, the isotherms without added PFAS become steeper and phase transitions from liquid-expanded (LE) to liquid-condensed (LC) phases were observed between 25-30 mN.[36] DMPC itself does not exhibit a LE-LC transition. The lift off pressure, which corresponds to the area per molecule when the surface pressure can be detected, also increased with DMPG concentration (~20% from X_{DMPG} = 0 to 0.3) due to repulsive electrostatic interactions between DMPG lipids that increased the effective mean lipid molecular area, Ā.[37]

With PFAS present in the subphase, the isotherms showed an increase in π after formation and equilibration at the highest mean molecular areas, Ā, reflecting the presence of PFAS at the interface. The effect was most pronounced for PFOS, which showed the greatest surface activity (Figure 1a-c). The presence of anionic PFAS added to the electrostatic repulsion within the monolayers originating with DMPG and altered the inter-lipid interactions that led to the LE-LC phase transition.

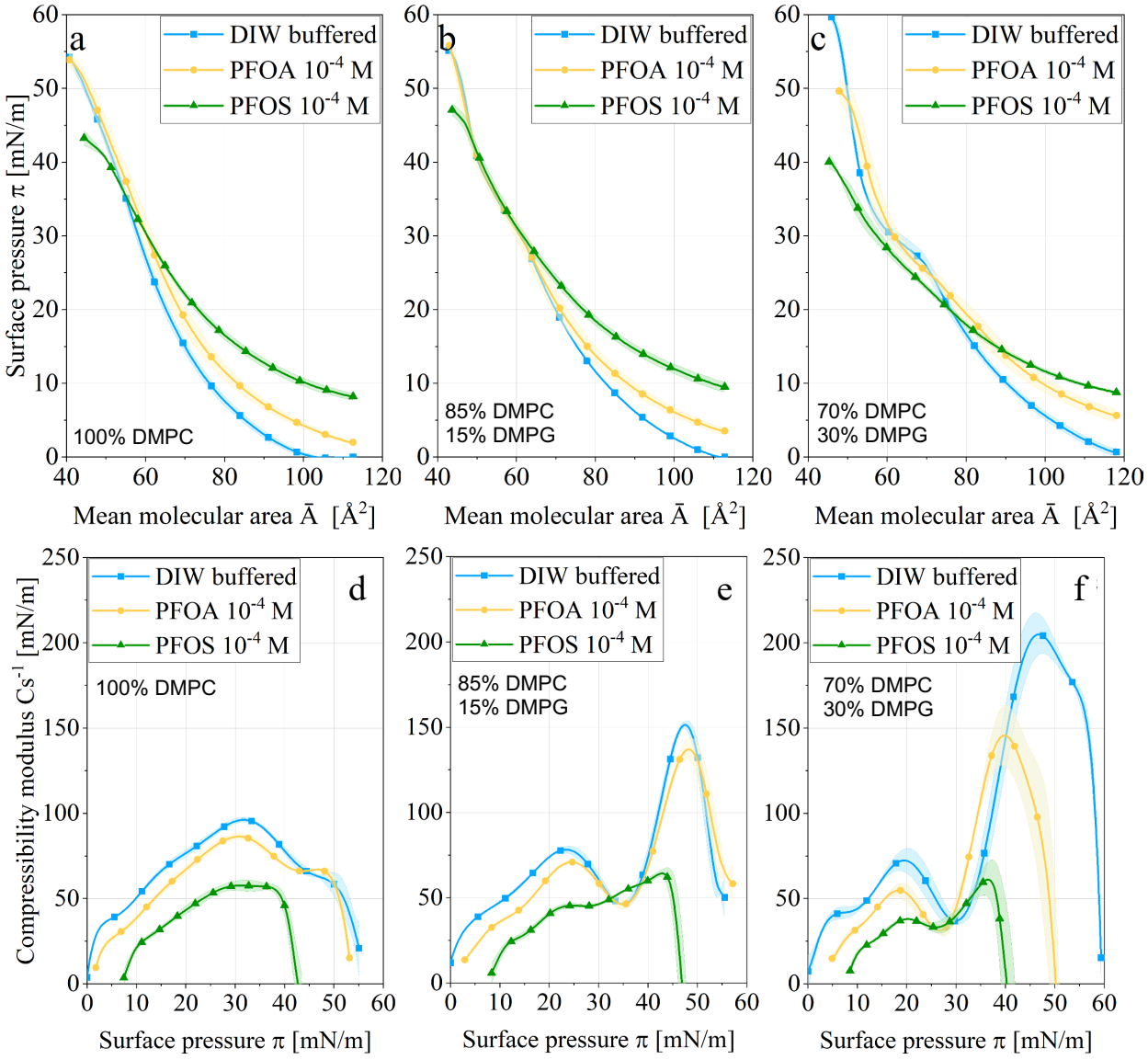

198

199 **Figure 1.** Surface pressure–area isotherms, π –Ā (a-c), and compressibility moduli, C_s^{-1} (d-f), for

200 DMPC monolayers as a function of DMPG concentration (X_{DMPG}) in the absence (blue squares)

201 or presence of 10^{-4} M PFOA (yellow circles) or PFOS (green triangles) in a HEPES buffered

202 DIW subphase. a, d) $X_{DMPG} = 0$; b, e) $X_{DMPG} = 0.15$; and c, f) $X_{DMPG} = 0.3$. The colored bands

203 shown in a-f for each condition represent the standard error of three independent experiments.

204

The isotherms with added PFAS were less steep upon compression, implying a more compressible monolayer, and intersected the phospholipid isotherms. Results for the compressibility moduli, C_s^{-1}, are shown in Figure 1d-f. The local minima near ~30–35 mN/m for X_{DMPG} at 0.15 and 0.3 represent π at the midpoint of the LE-LC phase transition. The minima are followed by rapid increases in C_s^{-1} (decreases in compressibility) as the structured LC phase formed.[20] Increasing DMPG concentrations led to decreases in C_s^{-1} when the monolayers were in the LE phase (more compressible) and increases C_s^{-1} in the LC phase (less compressible) at high surface pressures. This behavior is tied to DMPG, which reduced lipid packing in the LE phase via electrostatic repulsion and drove the LE-LC phase transition. The addition of PFAS to the subphase led to overall decreases in the compressibility moduli, with the decreases being more pronounced with increasing DMPG concentration. PFOS had a greater influence on C_s^{-1} because it is larger and more hydrophobic (Table 1, reflected in C_{nF}), and has greater surface activity than PFOA.

The effect of PFOA and PFOS on the LE-LC lipid phase transitions are revealed through the compressibility moduli. Only at the highest DMPG mole fraction, $X_{DMPG} = 0.3$ (Figure 1f), did we observe a shift in the transition to lower π and $\bar{A}$, consistent with a lipid condensing effect caused by the PFAS. Lipid condensation has been reported Lv and Sun,[39] where molecular dynamics simulations revealed that saturated 1,2-dipalmitoyl-*sn*-glycero-3-phosphocholine (DPPC, C_n:cis = 16:0) in a bilayer condense around PFOS to shield it from water, yielding a more thermodynamically favorably state. Since DMPC (C_n:cis = 14:0) does not exhibit a LE-LC transition alone, we only observed this condensing effect with DMPG was present.

To examine the effective area occupied by PFAS initially and the likelihood of PFAS exclusion at high compression, we determined the limiting area at high $\bar{A}$ (LE phase) and the

maximum surface pressure, respectively. The limiting area, expressed as the difference in limiting areas with and without added PFASs ($\bar{A}_{LP,min} - \bar{A}_{L,min}$), are shown in Figure 2a. The values increase with DMPG concentration, denoting the role of electrostatic repulsion in monolayer expansion. The values of $\bar{A}_{LP,min} - \bar{A}_{L,min}$ are an significantly lower than the estimated and computed PFAS area per headgroup shown in Table 2, suggesting that the PFAS aligned with the lipid tails and/or condensed surrounding lipids to reduce the mean lipid area per molecule.

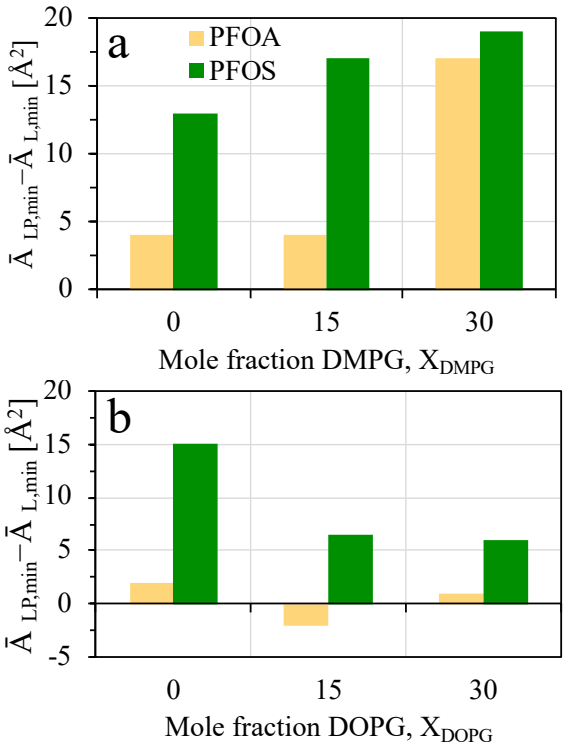

Figure 2. Difference in limiting areas with and without added PFOA or PFOS ($\bar{A}_{LP,min} - \bar{A}_{L,min}$) for a) DMPC/DMPG and b) DOPC/DOPG monolayers as a function PG lipid mole fraction. These values were taken from the mean isotherms.

240 Maximum surface pressures, π_{max}, are shown as a function of PG concentration in Figure
241 3. The labels 'c' and 'p' denote whether the maximum refers to a collapse (an abrupt drop in π
242 with compression at low Ā) or a plateau, with little to no evidence of collapse, respectively.
243 PFOA did not lower π_{max} at $X_{DMPG} = 0$ or 0.15, and at $X_{DMPG} = 0.3$ the decrease in π_{max} suggests
244 that the phospholipids did not pack tightly enough to 'squeeze' PFOA out of the monolayer due
245 to headgroup repulsion. However, a significant decrease in the collapse and plateau pressures
246 were observed for PFOS. These results indicate that PFOA was partially expelled from the
247 monolayers at high compression while PFOS remains within the monolayers, consistent with
248 PFOS showing greater phospholipid bilayer partitioning than PFOA.[2,3] The decrease of the
249 collapse pressure with a PFOS-rich subphase can be explained by the comparably high surface
250 activity, which leads to disordering effects due to disrupted inter-phospholipid interactions,
251 namely van der Waals attraction.[38] This phenomenon is coupled with increased electrostatic
252 repulsion within the monolayer due to PFOS, which restricts compression at low Ā resulting in
253 collapse.

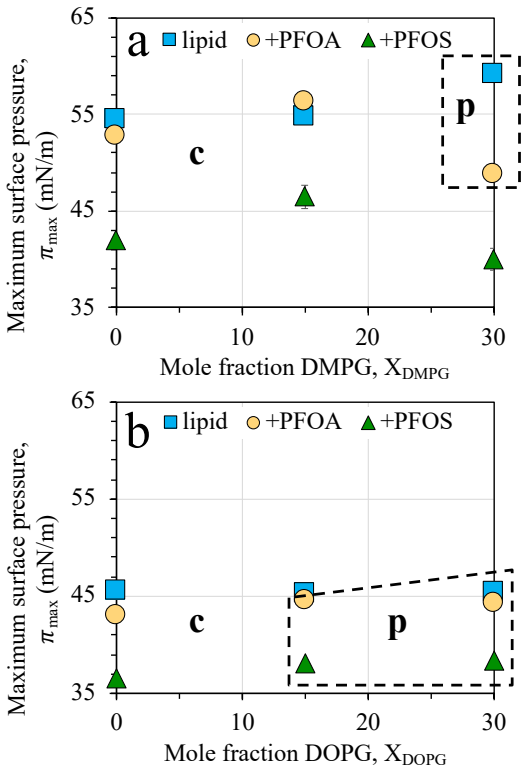

Figure 3. Maximum surface pressure, π_{max}, as a function of PG lipid concentration for a) DMPC/DMPG and b) DOPC/DOPG with added PFOA or PFOS. The labels 'c' and 'p' denote whether π_{max} refers to a collapse or a plateau (dashed rectangle shows plateau region). Standard error bars are shown based on triplicate measurements. Error bars not visible are smaller than the symbols.

BAM images of the monolayers compressed to 40 mN/m with X_{PG} = 0 and 0.3 are shown in Figure 4A. PFOA and PFOS led to the formation of bright 'spots' within DMPC monolayers (X_{DMPG} = 0) indicative of condensed, solid domains that are thicker than the surrounding bulk lipid phase. These solid domains became more prevalent with increasing π and were only observed with added PFAS. Phospholipid condensation observed by BAM and by $\bar{A}_{LP,min} - \bar{A}_{L,min}$ (Figure 2a) for DMPC monolayers support this mechanism. At X_{DMPG} = 0.3 condensation

could not be discerned as the solid phases were observed with and without added PFAS. Phospholipid condensation is typically associated with a stiffer or less compressible (higher C_s^{-1}) monolayer as opposed to a more compressible monolayer (Figure 1d-f). Thus, PFOA and PFOS have anomalous affects – they condense phospholipid domains while still fluidizing the monolayer and rendering it more compressible.

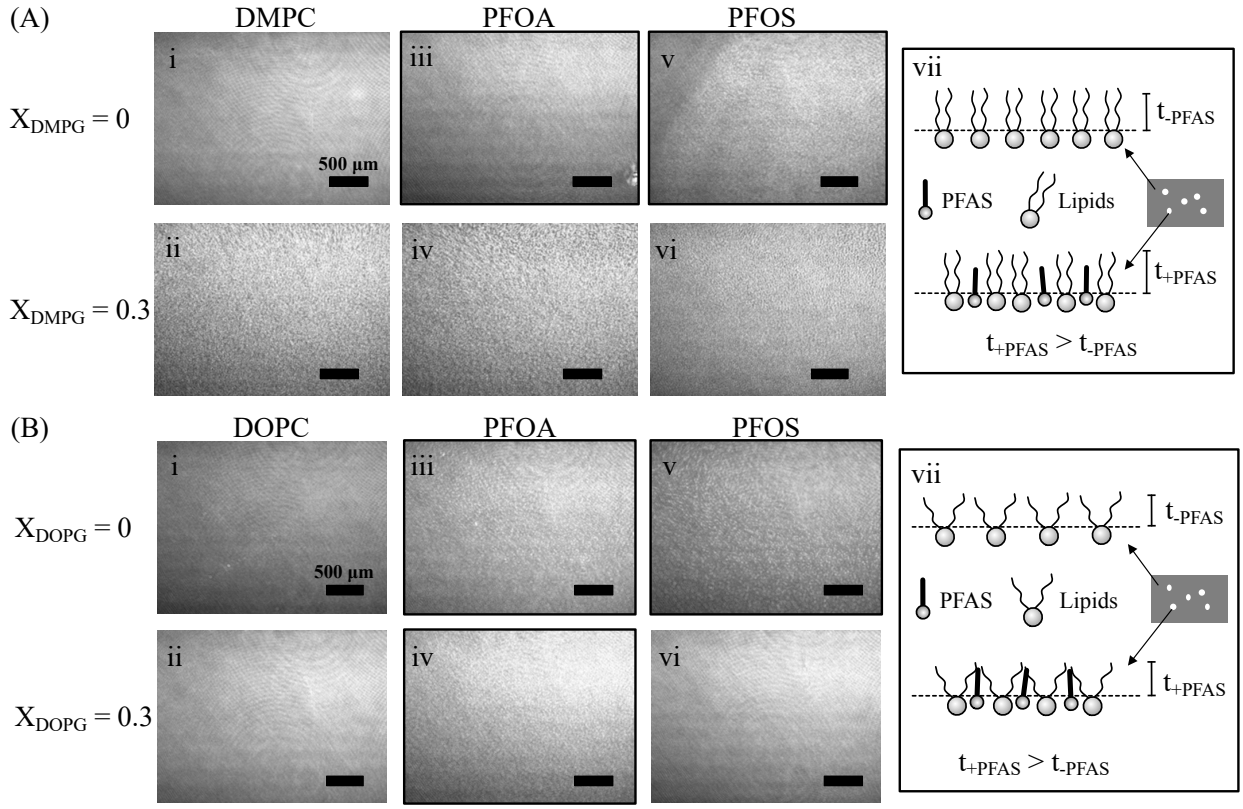

Figure 4. Brewster Angle Microscopy (BAM) images of (A) DMPC ($X_{DMPG} = 0$; i, iii, v) and DMPC/DMPG ($X_{DMPG} = 0.3$; ii, iv, vi) monolayers at 40 mN/m and (B) DOPC ($X_{DOPG} = 0$; i, iii, v) and DOPC/DOPG ($X_{DOPG} = 0.3$; ii, iv, vi) monolayers at 35 mN/m with added PFOA and PFOS. The same scale is used for each image and monolayers exhibiting lipid condensation are shown as images with black line border. Proposed schematics are shown (not to scale; vii) depicting lipid condensation in the presence of PFAS.

Viada et al[40] have reported that perfluorodecanoic acid (PFDA) is expelled at high compression from anionic distearoylphosphatidic acid (DSPA) monolayers where the difference in lipid tail length to C_{nF} is 9 carbon atoms, but mixes within dilauroylphosphatidic acid (DLPA) monolayers where the difference is 3 carbon atoms. DSPA and DLPA both contain saturated tails. Comparatively, the tail length difference for PFOA and PFOS with DM lipids is 6 and 7 carbon atoms, respectively. This comparison shows that small changes in PFAS length – one carbon atom – may determine whether PFAS are retained within or expelled from phospholipid monolayers. Headgroup chemistry likely plays an important role as well and the ability for PFOS to be retained within the monolayer could stem from stronger hydrogen bonding between the sulfonic acid headgroup and the lipid headgroups.

3.2. Unsaturated Phospholipid Monolayers (DOPC and DOPC/DOPG)

The DOPC isotherm shows good agreement with the literature[41] and with DOPG, monotonic increases in π are observed with compression with no evidence of LE-LC phase transitions (expected for lipids with unsaturated tails; Figure 5a-c). The DOPC/DOPG isotherms exhibit much of the same behavior observed for DMPC/DMPG, with greater lift-off areas with increasing X_{DOPG}, (~6% from X_{DOPG} = 0 to 0.3) and, with PFAS present, PFOS having the greatest effect on the isotherm. This similarity for lipids with short/saturated and long/unsaturated tails shows the importance of electrostatic interactions between lipid and PFAS headgroups.

The *cis* double bond in DOPC and DOPG tails leads to a fluid monolayer with low packing densities compared to saturated lipids. This is reflected in the compressibility moduli shown in Figure 5d-f. Interestingly, C_s^{-1} for DOPC or DOPC/DOPG mixtures do not show

303 significant differences without added PFAS. Both PFAS reduced C_s^{-1} (increased compressibility)
304 compared to the pure lipid, however with added PFAS the C_s^{-1} profiles increased with increasing
305 X_{DOPG} (decreased compressibility). Compared to DMPC/DMPG, these results suggest that
306 DOPC/DOPG can more easily accommodate the PFAS with the void space provided by
307 unsaturated tails, reducing the impact of unfavorable electrostatic repulsion. Since PFAS
308 partitioned into these void spaces, there was less of an effect on the compressibility as the lipid
309 heads are spaced apart by the unsaturated lipid tails. The proposed mechanism is supported by
310 the differences in minimum area, showing that PFASs occupy a lower effective area compared to
311 DMPC/DMPG (Figure 2), and the π_{max} (Figure 3), showing that less PFAS is excluded from the
312 monolayer upon collapse or plateau.
313

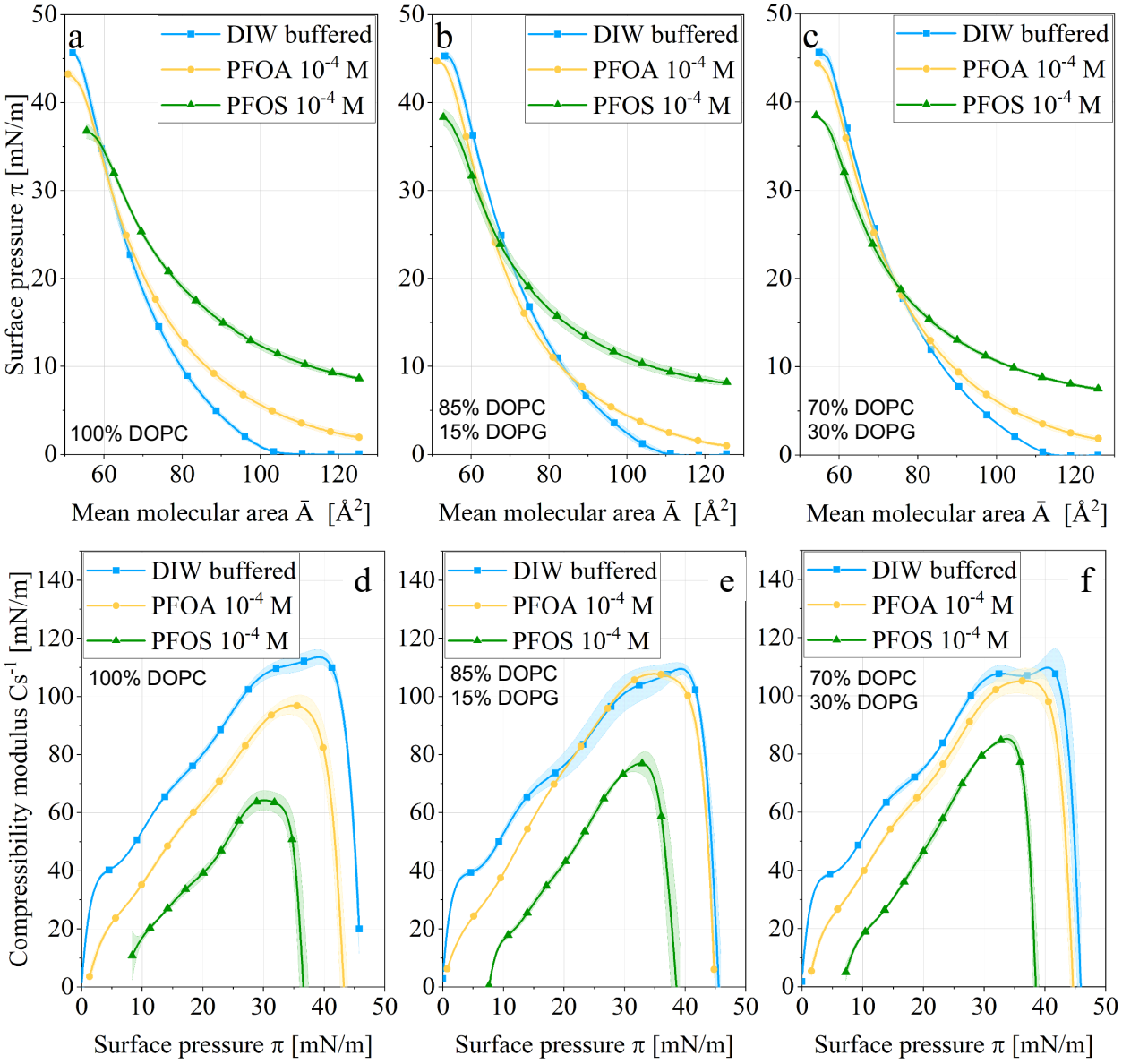

Figure 5. Surface pressure–area isotherms, π –Ā (a-c), and compressibility moduli, C_s^{-1} (d-f), for DOPC monolayers as a function of DOPG concentration (X_{DOPG}) in the absence (blue squares) or presence of 10^{-4} M PFOA (yellow circles) or PFOS (green triangles). a, d) $X_{DOPG} = 0$; b, e) $X_{DOPG} = 0.15$; and c, f) $X_{DOPG} = 0.3$. The colored bands shown in a-f for each condition represent the standard error of three independent experiments.

Like DMPC, BAM images show the PFOA and PFOS can lead to condensed solid domains in DOPC monolayers (Figure 4B) despite unfavorable lipid packing of the DOPC acyl tails. There was also evidence of PFOA causing condensation in DOPC/DOPG (X_{DOPG} = 0.3) monolayers, which are not known to form LC domains. Experimental results for DOPC support recent molecular dynamic simulations showing that PFOA and PFOS cause unsaturated lipids to condense in a bilayer.[42]

To examine whether electrostatic repulsion would prevent PFAS partitioning into net anionic monolayers, experiments were conducted where PFOS was added to the subphase with preexisting PC and PC/PG (X_{PG} = 0.3) monolayers at the air/water interface and the relative dynamic surface pressure, π/π_0 (initial surface pressure π_0 =35 mN/m), was measured over 8 h. In all cases the addition of PFOS led to an increase in π/π_0 compared to the PFOS-free condition over the duration of the experiments (Figure S6). This indicates that PFOS penetrated the monolayer and led to increased lipid packing at the interface, which increased π irrespective of the net-charge of the monolayer or lipid tail saturation. The effect of PFOS on was less pronounced for monolayers with unsaturated lipids, further supporting the proposed mechanism of PFAS adsorption in void space at the interface.

3.3. Extracted Bacterial Lipid Monolayers

The major classes of lipids identified in the bacterial lipid extracts were phosphatidylglycerols (PG; 46.8 ± 0.5%), phosphatidylethanolamine (PE; 33.7 ± 0.8%), and glyceroglycolipids (18.3 ± 0.2%). LysoPE and phosphatidic acid (PA) were also present at 0.6 ± 0.1% each. The abundant species of PE and PG lipids had a total of 32 or 34 carbon atoms; 32 carbon atoms likely correspond to lipids with two C_{16} tails or one C_{14} and one C_{18} tail, while 34

carbon atoms likely corresponded to one C_{16} tail and one C_{18} tail. For both species there were 1 or 2 degrees of fatty acid tail unsaturation (double bonds). For comparison, DMPC contains two saturated C_{14} tails and DOPC contains two C_{18} tails, each with a double bond between C_9=C_{10} that leads to void space for PFAS adsorption within a monolayer.

For Langmuir trough studies on model bacterial lipid monolayers the range of PFAS was expanded to include PFHxS (C_{nF} = 6) and PFNA (C_{nF} = 8), in addition to PFOS (C_{nF} = 8) and PFOA (C_{nF} = 7). Bacterial lipid monolayer isotherms display properties of both DMPC/DMPG and DOPC/DOPG. Without PFAS, a transition from a less-ordered to a more-ordered phase is observed from ~15-25 mN/m (Figure 6; the transition cannot be defined as LE-LC) and the monolayer is highly compressible (low C_s^{-1}; Figure S7).

With added PFASs, π after initial monolayer formation increased with increasing PFAS concentration and the monolayers were more fluid and compressible. The isotherms with PFNA and PFOS are very similar (Figures 6b and d, respectively), suggesting that PFASs interactions within the monolayer are due to length of the fluorinated tail for these PFAS with C_{nF} = 8 and that the effect of the headgroup, carboxylic vs sulfonic acid, is small in comparison. This is consistent with the similar surface activities measured for PFNA and PFOS (Figure S5). The intersections of the isotherms are shifted to larger areas with increasing concentrations, consistent with increased headgroup electrostatic repulsion that reflects the charge of PFAS and the high concentration of negative PG lipids in the bacterial lipid monolayers.

Fluorinated tail length does not however explain the differences observed for PFOA and PFHxS. With PFOA (C_{nF} = 7; Figure 6c) there was almost no change in the isotherms, while the shorter PFHxS (C_{nF} = 6; Figure 6a) led to an expanded and more compressible monolayer. The less-ordered to more-ordered phase transition also became more pronounced with increasing

PFHxS concentration. Comparatively, PFNA and PFOS inhibited the phase transition, and PFOA had no effect.

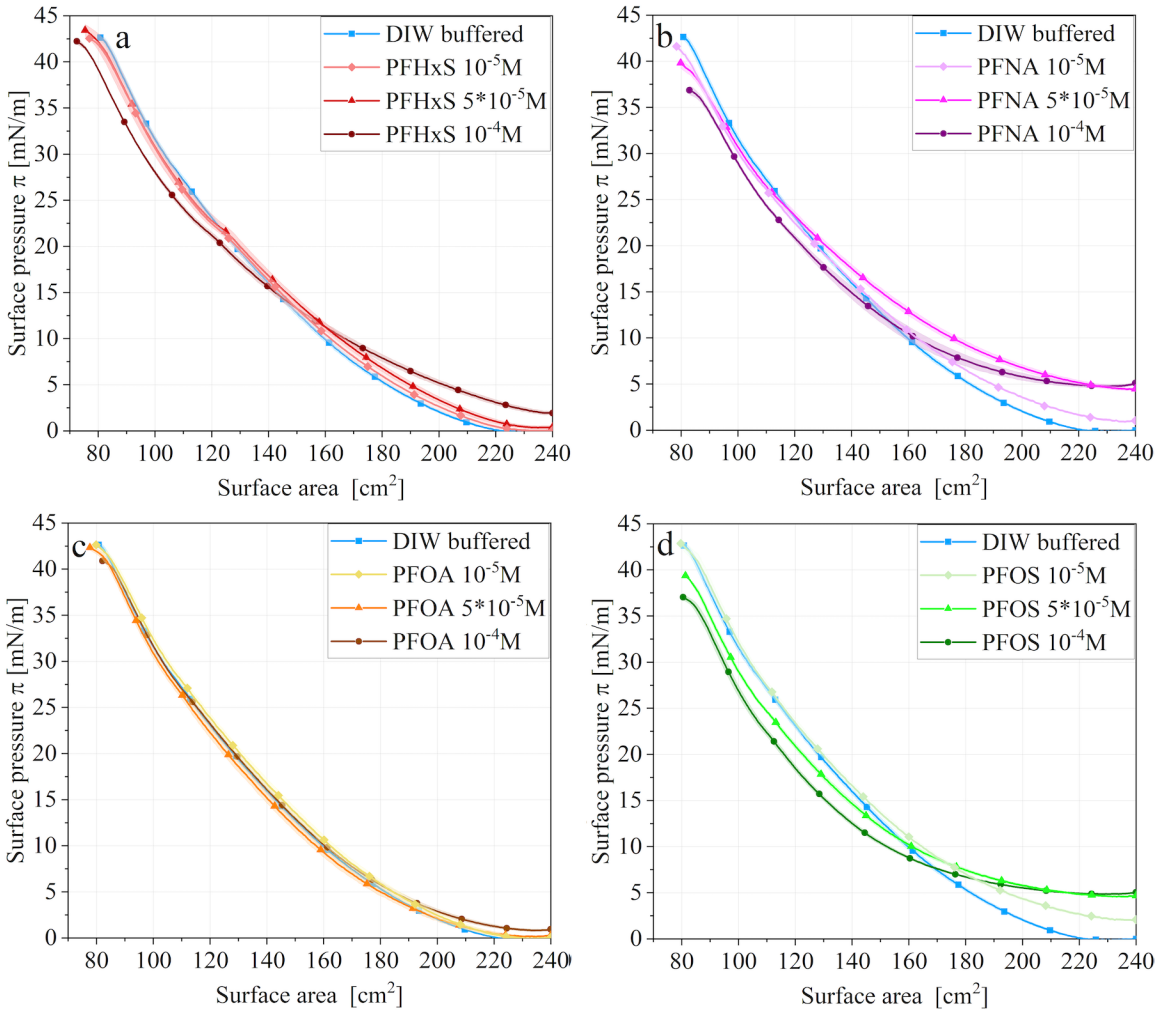

Figure 6. Surface pressure–area (π –A) isotherms for extracted bacterial lipid monolayers in the absence or presence of a) PFHxS, b) PFNA, c) PFOA, and d) PFOS as a function of PFAS concentration. The colored bands shown in a-f for each condition represent the standard error of three independent experiments.

PFHxS is an interesting molecule compared to similar PFAS. Albumin binding studies have shown that PFAS partition coefficients increase with increasing number of fluorinated

carbons with the exception of PFHxS, which exhibited greater protein binding.[43] The half-life of PFHxS in humans is also greater than expected based on C_{nF}.[44] These studies suggest that PFHxS may exhibit more hydrophobic behavior than expected, which would explain its high surface activity (Figure S5) despite its high water solubility compared to the other PFAS examined.[33]

Monolayer collapse occurs when a monolayer becomes tightly packed and unstable, which leads to buckling or the formation of multilayer regions at a liquid interface. For bacterial lipid monolayers, the surface pressure upon collapse decreased linearly with increasing PFOA, PFNA, and PFOS concentrations in the subphase (Figure 7), with PFNA and PFOS being nearly identical. A decrease in the collapse surface pressure reflects additional electrostatic repulsion due to the presence of PFAS in the monolayer that prevents the lipids from packing as tightly at the point of collapse. The collapse pressure is similar to DOPC/DOPG for these three PFAS at 10^{-4} M (Figure 5). PFHxS is again an anomaly – despite fluidizing the monolayer, the collapse pressure differed by just ~0.4 mN/m from the control and did not change with PFHxS concentration.

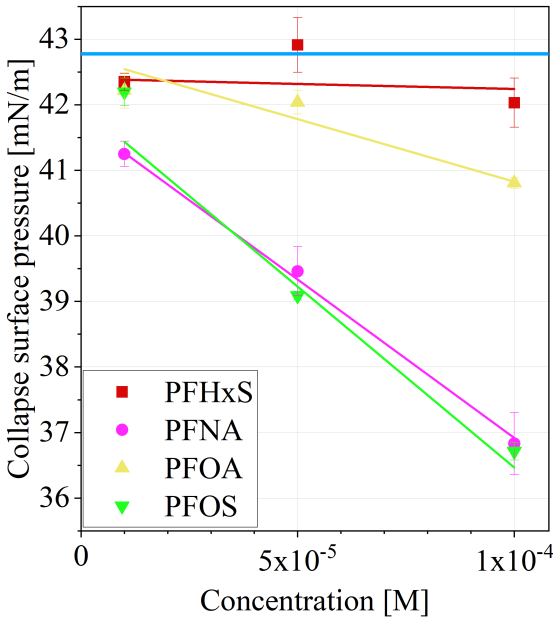

Figure 6. Collapse surface pressure of bacterial lipid monolayers as a function of PFAS subphase concentration. The blue horizontal line is the collapse pressure at 42.8 mN/m of the monolayers without PFAS. Standard error bars are shown based on triplicate measurements. Error bars not visible are smaller than the symbols.

A clear dissimilarity between the bacterial and synthetic lipid monolayers was observed when dynamic π/π_0 was measured for the bacterial lipid monolayers when PFAS was injected into the subphase. PFOS as well as PFHxS, PFOA, and PFNA had little effect on π over 8 h, suggesting that high content of negatively charged lipid (47.4 mol% PG + PA) and unsaturated lipid tails provided ample void space (high effective area per lipid) for PFAS to adsorb at the air/water interface without packing the lipids. This was observed to a lesser extent for DOPC/DOPG with increasing PG lipid content up to 30 mol%. There was no clear BAM evidence of PFAS causing lipid condensation in the bacterial lipid monolayers.

4. Conclusions

The ability of the PFAS examined to disrupt synthetic phospholipid and bacterial lipid monolayers was dependent on the extent to which it was retained within the monolayer during compression and the ability for the monolayer accommodate the PFAS in void spaces caused by unsaturated lipids. PFOA was partially expelled from the monolayers at high compression where the more hydrophobic PFOS was retained and contributed an additional repulsive interaction that ultimately led to more fluid, compressible monolayer that collapsed with less force. By combining BAM and isotherm results, experimental evidence confirmed prior computational results showing that PFAS can cause phospholipid condensation. Interestingly, we observed that

PFOA and PFOS caused lipid condensation while still yielding a more fluid, compressible monolayer. Other molecules such as cholesterol that cause lipid condensation also increase the rigidity and reduce the compressibility of lipid monolayers.

The effects of PFAS on the fluidity and compressibility of synthetic monolayers were also observed for extracted bacterial membrane monolayers. For the bacterial lipid monolayers, PFOS and PFNA, a sulfonic acid and a carboxylic acid both with C_8 fluorinated tails, fluidized the monolayers and led to early monolayer collapse. PFOA and PFHxS had comparably modest effects. Given the thousands of PFAS present in our environment, additional studies are needed to determine if the interactions observed in this work can be extended to classes of PFAS as well as other PFAS structures (e.g. cationic PFAS or PFAS precursors), and if similar effects of are observed for other environmentally relevant bacterial membranes.

Acknowledgements

This work was funded by the National Institute of Environmental Health Science Sources, Transport, Exposure & Effects of PFASs (STEEP) Superfund Research Program under grant P42ES027706. STEEP is a partnership of the University of Rhode Island, the Harvard T.H. Chan School of Public Health Department of Environmental Health, and the Silent Spring Institute. The lipid analyses described in this work were performed at the Kansas Lipidomics Research Center Analytical Laboratory. Instrument acquisition and lipidomics method development were supported by the National Science Foundation (including support from the Major Research Instrumentation program; most recent award DBI-1726527), K-IDeA Networks of Biomedical Research Excellence (INBRE) of National Institute of Health (P20GM103418), USDA National Institute of Food and Agriculture (Hatch/Multi-State project 1013013), and

Kansas State University. We are grateful to Bongsup Cho, Daniel Roxbury, and Sigrid Berka for their valuable insight.

References

(1) Ghisi, R.; Vamerali, T.; Manzetti, S. Accumulation of Perfluorinated Alkyl Substances (PFAS) in Agricultural Plants: A Review. *Environ. Res.* **2019**, *169*, 326–341.

(2) Pérez, F.; Nadal, M.; Navarro-Ortega, A.; Fàbrega, F.; Domingo, J. L.; Barceló, D.; Farré, M. Accumulation of Perfluoroalkyl Substances in Human Tissues. *Environ. Int.* **2013**, *59*, 354–362.

(3) Kwiatkowski, C. F.; Andrews, D. Q.; Birnbaum, L. S.; Bruton, T. A.; DeWitt, J. C.; Knappe, D. R. U.; Maffini, M. V.; Miller, M. F.; Pelch, K. E.; Reade, A.; et al. Scientific Basis for Managing PFAS as a Chemical Class. *Environ. Sci. Technol. Lett.* **2020**, *7* (8), 532–543.

(4) Fiedler, S.; Pfister, G.; Schramm, K.-W. Poly- and Perfluorinated Compounds in Household Consumer Products. *Toxicol. Environ. Chem.* **2010**, *92* (10), 1801–1811.

(5) Kotthoff, M.; Müller, J.; Jürling, H.; Schlummer, M.; Fiedler, D. Perfluoroalkyl and Polyfluoroalkyl Substances in Consumer Products. *Environ. Sci. Pollut. Res.* **2015**, *22* (19), 14546–14559.

(6) Fujii, S.; Polprasert, C.; Tanaka, S.; Hong Lien, N. P.; Qiu, Y. New POPs in the Water Environment: Distribution, Bioaccumulation and Treatment of Perfluorinated Compounds – a Review Paper. *J. Water Supply Res. Technol.* **2007**, *56* (5), 313–326.

(7) Huang, R.; Chen, Q.; Zhang, L.; Luo, K.; Chen, L.; Zhao, S.; Feng, L.; Zhang, J. Prenatal Exposure to Perfluoroalkyl and Polyfluoroalkyl Substances and the Risk of Hypertensive

Disorders of Pregnancy. *Environ. Heal.* **2019**, *18* (1), 5.

(8) Post, G. B.; Gleason, J. A.; Cooper, K. R. Key Scientific Issues in Developing Drinking Water Guidelines for Perfluoroalkyl Acids: Contaminants of Emerging Concern. *PLOS Biol.* **2017**, *15* (12), e2002855.

(9) Rotander, A.; Toms, L.-M. L.; Aylward, L.; Kay, M.; Mueller, J. F. Elevated Levels of PFOS and PFHxS in Firefighters Exposed to Aqueous Film Forming Foam (AFFF). *Environ. Int.* **2015**, *82*, 28–34.

(10) Reth, M.; Berger, U.; Broman, D.; Cousins, I. T.; Nilsson, E. D.; McLachlan, M. S. Water-to-Air Transfer of Perfluorinated Carboxylates and Sulfonates in a Sea Spray Simulator. *Environ. Chem.* **2011**, *8* (4), 381.

(11) Kwok, K. Y.; Yamazaki, E.; Yamashita, N.; Taniyasu, S.; Murphy, M. B.; Horii, Y.; Petrick, G.; Kallerborn, R.; Kannan, K.; Murano, K.; et al. Transport of Perfluoroalkyl Substances (PFAS) from an Arctic Glacier to Downstream Locations: Implications for Sources. *Sci. Total Environ.* **2013**, *447*, 46–55.

(12) Dassuncao, C.; Pickard, H.; Pfohl, M.; Tokranov, A. K.; Li, M.; Mikkelsen, B.; Slitt, A.; Sunderland, E. M. Phospholipid Levels Predict the Tissue Distribution of Poly- and Perfluoroalkyl Substances in a Marine Mammal. *Environ. Sci. Technol. Lett.* **2019**, *6* (3), 119–125.

(13) Ng, C. A.; Hungerbühler, K.; Hungerbuhler, K. Bioaccumulation of Perfluorinated Alkyl Acids: Observations and Models. *Env. Sci Technol* **2014**, *48* (9), 4637–4648.

(14) Ng, C. A.; Hungerbühler, K. Bioconcentration of Perfluorinated Alkyl Acids: How Important Is Specific Binding? *Environ. Sci. Technol.* **2013**, *47* (13), 7214–7223.

(15) Ngyugen, H.; McNamee, C. E. Determination and Comparison of How the Chain Number

and Chain Length of a Lipid Affects Its Interactions with a Phospholipid at an Air/Water Interface. *J. Phys. Chem. B* **2014**, *118* (22), 5901–5912.

(16) Xie, W.; Ludewig, G.; Wang, K.; Lehmler, H.-J. J. Model and Cell Membrane Partitioning of Perfluorooctanesulfonate Is Independent of the Lipid Chain Length. *Colloids and Surfaces B-Biointerfaces* **2010**, *76* (1), 128–136.

(17) Nouhi, S.; Ahrens, L.; Campos Pereira, H.; Hughes, A. V.; Campana, M.; Gutfreund, P.; Palsson, G. K.; Vorobiev, A.; Hellsing, M. S. Interactions of Perfluoroalkyl Substances with a Phospholipid Bilayer Studied by Neutron Reflectometry. *J. Colloid Interface Sci.* **2018**, *511*, 474–481.

(18) Oldham, E. D.; Xie, W.; Farnoud, A. M.; Fiegel, J.; Lehmler, H.-J. J. Disruption of Phosphatidylcholine Monolayers and Bilayers by Perfluorobutane Sulfonate. *J Phys Chem B* **2012**, *116* (33), 9999–10007.

(19) Matyszewska, D.; Bilewicz, R. Influence of Perfluorinated Compounds on Model Lipid Membranes Prepared Using Langmuir and Langmuir–Schaefer Techniques. *Colloids Surfaces A Physicochem. Eng. Asp.* **2008**, *321* (1–3), 11–15.

(20) Matyszewska, D.; Tappura, K.; Orädd, G.; Bilewicz, R. Influence of Perfluorinated Compounds on the Properties of Model Lipid Membranes. *J. Phys. Chem. B* **2007**, *111* (33), 9908–9918.

(21) Lehmler, H.-J. J.; Xie, W.; Bothun, G. D.; Bummer, P. M.; Knutson, B. L. Mixing of Perfluorooctanesulfonic Acid (PFOS) Potassium Salt with Dipalmitoyl Phosphatidylcholine (DPPC). *Coll. Surf. B* **2006**, *51* (1), 25–29.

(22) Xie, W.; Bothun, G. D.; Lehmler, H.-J. J. Partitioning of Perfluorooctanoate into Phosphatidylcholine Bilayers Is Chain Length-Independent. *Chem. Phys. Lipids* **2010**, *163*

(3), 300–308.

(23) Fitzgerald, N. J. M.; Wargenau, A.; Sorenson, C.; Pedersen, J.; Tufenkji, N.; Novak, P. J.; Simcik, M. F. Partitioning and Accumulation of Perfluoroalkyl Substances in Model Lipid Bilayers and Bacteria. *Environ. Sci. Technol.* **2018**, *52* (18), 10433–10440.

(24) Fitzgerald, N. J. M.; Simcik, M. F.; Novak, P. J. Perfluoroalkyl Substances Increase the Membrane Permeability and Quorum Sensing Response in Aliivibrio Fischeri. *Environ. Sci. Technol. Lett.* **2018**.

(25) Liu, G.; Zhang, S.; Yang, K.; Zhu, L.; Lin, D. Toxicity of Perfluorooctane Sulfonate and Perfluorooctanoic Acid to Escherichia Coli: Membrane Disruption, Oxidative Stress, and DNA Damage Induced Cell Inactivation and/or Death. *Environ. Pollut.* **2016**.

(26) Weathers, T. S.; Higgins, C. P.; Sharp, J. O. Enhanced Biofilm Production by a Toluene-Degrading Rhodococcus Observed after Exposure to Perfluoroalkyl Acids. *Environ. Sci. Technol.* **2015**, *49* (9), 5458–5466.

(27) Yakimov, M. M.; Golyshin, P. N.; Lang, S.; Moore, E. R. B.; Abraham, W.-R.; Lunsdorf, H.; Timmis, K. N. Alcanivorax Borkumensis Gen. Nov., Sp. Nov., a New, Hydrocarbon-Degrading and Surfactant-Producing Marine Bacterium. *Int. J. Syst. Bacteriol.* **1998**, *48* (2), 339–348.

(28) Schneiker, S.; dos Santos, V. A. M.; Bartels, D.; Bekel, T.; Brecht, M.; Buhrmester, J.; Chernikova, T. N.; Denaro, R.; Ferrer, M.; Gertler, C.; et al. Genome Sequence of the Ubiquitous Hydrocarbon-Degrading Marine Bacterium Alcanivorax Borkumensis. *Nat. Biotechnol.* **2006**, *24* (8), 997–1004.

(29) Konieczna, M.; Olzog, M.; Naether, D.; Chrzanowski, Ł.; Heipieper, H. Membrane Fatty Acid Composition and Cell Surface Hydrophobicity of Marine Hydrocarbonoclastic

Alcanivorax Borkumensis SK2 Grown on Diesel, Biodiesel and Rapeseed Oil as Carbon Sources. *Molecules* **2018**, *23* (6), 1432.

(30) USEPA. CompTox Chemicals Dashboard https://comptox.epa.gov/dashboard/.

(31) Anaya, N. M.; Faghihzadeh, F.; Ganji, N.; Bothun, G.; Oyanedel-Craver, V. Comparative Study between Chemostat and Batch Reactors to Quantify Membrane Permeability Changes on Bacteria Exposed to Silver Nanoparticles. *Sci. Total Environ.* **2016**, *565*, 841–848.

(32) Bligh, E. G.; Dyer, W. J. A Rapid Method of Total Lipid Extraction and Purification. *Can. J. Biochem. Physiol.* **1959**, *37* (8), 911–917.

(33) Kim, M.; Li, L. Y.; Grace, J. R.; Yue, C. Selecting Reliable Physicochemical Properties of Perfluoroalkyl and Polyfluoroalkyl Substances (PFASs) Based on Molecular Descriptors. *Environ. Pollut.* **2015**, *196* (May 2009), 462–472.

(34) Schaefer, C. E.; Culina, V.; Nguyen, D.; Field, J. Uptake of Poly- and Perfluoroalkyl Substances at the Air–Water Interface. *Environ. Sci. Technol.* **2019**, *53* (21), 12442–12448.

(35) Costanza, J.; Arshadi, M.; Abriola, L. M.; Pennell, K. D. Accumulation of PFOA and PFOS at the Air–Water Interface. *Environ. Sci. Technol. Lett.* **2019**, *6* (8), 487–491.

(36) Park, C. K.; Schmitt, F. J.; Evert, L.; Schwartz, D. K.; Israelachvili, J. N.; Knobler, C. M. Film Balance and Fluorescence Microscopic Investigation of the Effects of Ca2+ on Mixed DMPC/DMPG Monolayers. *Langmuir* **1999**, *15* (1), 202–206.

(37) Vernoux, N.; Maniti, O.; Besson, F.; Granjon, T.; Marcillat, O.; Vial, C. Mitochondrial Creatine Kinase Adsorption to Biomimetic Membranes: A Langmuir Monolayer Study. *J. Colloid Interface Sci.* **2007**, *310* (2), 436–445.

(38) Boggs, J. M. Lipid Intermolecular Hydrogen Bonding: Influence on Structural Organization and Membrane Function. *Biochim. Biophys. Acta - Rev. Biomembr.* **1987**, *906* (3), 353–404.

(39) Lv, G.; Sun, X. The Molecular-Level Understanding of the Uptake of PFOS and Its Alternatives (6:2 Cl-PFESA and OBS) into Phospholipid Bilayers. *J. Hazard. Mater.* **2021**, *417*, 125991.

(40) Viada, B.; Cámara, C. I.; Yudi, L. M. Destabilizing Effect of Perfluorodecanoic Acid on Simple Membrane Models. *Soft Matter* **2019**, *15* (11), 2447–2462.

(41) Guzmán, E.; Liggieri, L.; Santini, E.; Ferrari, M.; Ravera, F. DPPC–DOPC Langmuir Monolayers Modified by Hydrophilic Silica Nanoparticles: Phase Behaviour, Structure and Rheology. *Colloids Surfaces A Physicochem. Eng. Asp.* **2012**, *413*, 174–183.

(42) Shen, Z.; Ge, J.; Ye, H.; Tang, S.; Li, Y. Cholesterol-like Condensing Effect of Perfluoroalkyl Substances on a Phospholipid Bilayer. *J. Phys. Chem. B* **2020**, *124* (26), 5415–5425.

(43) Allendorf, F.; Berger, U.; Goss, K.-U. U.; Ulrich, N. Partition Coefficients of Four Perfluoroalkyl Acid Alternatives between Bovine Serum Albumin (BSA) and Water in Comparison to Ten Classical Perfluoroalkyl Acids. *Environ. Sci. Process. Impacts* **2019**, *21* (11), 1852–1863.

(44) Olsen, G. W.; Burris, J. M.; Ehresman, D. J.; Froehlich, J. W.; Seacat, A. M.; Butenhoff, J. L.; Zobel, L. R. Half-Life of Serum Elimination of Perfluorooctanesulfonate, Perfluorohexanesulfonate, and Perfluorooctanoate in Retired Fluorochemical Production Workers. *Environ. Health Perspect.* **2007**, *115* (9), 1298–1305.